Pergamon

Chemical Engineering Science, Vol. 50, No. 16, pp. 2507–2522, 1995

0009-2509/95 $9.50 + 0.00

0009-2509(95)00102-6

EXPERIMENTAL VERIFICATION OF THE MAXWELL–STEFAN THEORY FOR MICROPORE DIFFUSION

L. J. P. VAN DEN BROEKE and R. KRISHNA†
Department of Chemical Engineering, University of Amsterdam, Nieuwe Achtergracht 166, 1018 WV Amsterdam, The Netherlands

(*First received* 23 *November* 1994; *revised manuscript received* 15 *February* 1995; *accepted* 21 *February* 1995)

Abstract—The main objective of this paper is to test the capability of the Maxwell–Stefan theory for predicting the diffusion behaviour of multicomponent mixtures within micropores on the basis of the diffusion behaviour of single components. Diffusion within micropores involves movement of sorbed species. It is an activated process. The proper driving force is the gradient of the surface chemical potential. In the Maxwell–Stefan theory for micropore diffusion, the adsorption sites on the surface are viewed as pseudo-species, analogous to craters on the surface of the moon. The surface coverage has a significant influence on the mass transfer fluxes. The Maxwell–Stefan theory yields alternative approaches to micropore diffusion as special cases and is consistent with the theory of irreversible thermodynamics. The Maxwell–Stefan diffusivity for signal-component diffusion $Đ$ is usually referred to as the "corrected" diffusivity in the literature. For binary diffusion, the Maxwell–Stefan equations, when combined with Langmuir adsorption equilibrium, coincide with the formulation derived by Habgood in 1958.

To test the predictive capability of the Maxwell–Stefan theory we performed breakthrough experiments with single components and mixtures containing methane, carbon dioxide, propane and propene. These experiments were carried out in a packed bed of microporous activated carbon and with carbon molecular sieves. It is clearly demonstrated that the mixture behaviour can be predicted by the Maxwell–Stefan theory extremely well under a wide range of conditions: co-adsorption, co-desorption and counter-sorption. A model in which the matrix of Fick diffusivities is assumed to be constant is shown to be less successful in this regard.

INTRODUCTION

A proper description of diffusion of multicomponent mixtures inside porous materials is essential in the simulation and design of catalytic reactors, adsorption and membrane separation processes (Froment and Bischoff, 1990; Kärger and Ruthven, 1992; Ruthven, 1984; Ruthven *et al.*, 1994; Wesselingh and Krishna, 1990; Yang, 1987). There is increasing interest in the use of microporous materials such as zeolites or carbon molecular sieves for separations (Kapteijn *et al.*, 1994a, b; Rao and Sircar, 1993).

Krishna (1990, 1993a, b) has recently developed a theory for micropore diffusion using the Maxwell–Stefan formulation and borrowing ideas and concepts from the dusty gas model (Mason and Malinauskas, 1983). The overall objective of this paper is to test the capability of the Maxwell–Stefan formulation of micropore diffusion to predict the diffusion behaviour of two, or more, components on the basis of information of single-component diffusion behaviour. Testing and validation of the Maxwell–Stefan approach is done on the basis of comparison of model predictions with experimental work in a fixed bed column with microporous carbon and carbon molecular sieves.

We begin with a summary of the Maxwell–Stefan theory for micropore diffusion.

MAXWELL–STEFAN THEORY FOR MICROPORE DIFFUSION

The dusty gas model approach (Mason and Malinauskas, 1983) can be adapted to the description of micropore diffusion by considering the vacant sites to be the $(n+1)$th pseudo-species in the (surface) system (Krishna, 1990, 1993a, b). Using the Maxwell–Stefan diffusion formulation as a basis and a simple mechanistic model pictured in Fig. 1 as theoretical guideline, the following expression to describe micropore diffusion can be derived:

$$-\nabla\mu_i = RT\sum_{j=1}^{n}\theta_j\frac{(\mathbf{v}_i-\mathbf{v}_j)}{Đ_{ij}} + RT\theta_{n+1}\frac{(\mathbf{v}_i-\mathbf{v}_{n+1})}{Đ_{i,n+1}},\quad i=1,2,\ldots,n. \quad (1)$$

Here $-\nabla\mu_i$, the surface chemical potential gradient, is the force acting on species i tending to move it along the surface. The first term on the right of eq. (1) reflects the friction exerted by adsorbate j on the surface motion of adsorbed species i. The second term reflects the friction experienced by the species i from the vacancies. The θ's in eq. (1) represent the fractional occupancies of the adsorbed species. Thus θ_i represents the fractional occupancy of the sites by the adsorbed species i and θ_{n+1} represent the fraction of unoccupied, vacant, sites,

$$\theta_{n+1} = 1-\theta_1-\theta_2-\cdots-\theta_n = 1-\theta_t. \quad (2)$$

†Author to whom correspondence should be addressed.

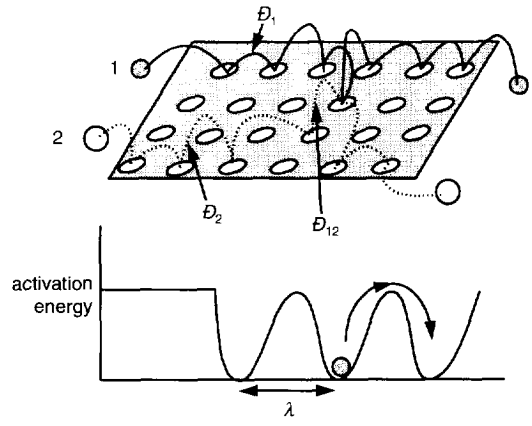

Fig. 1. A conceptual model for surface diffusion of adsorbed species 1 and 2. $Đ_1$ and $Đ_2$ are the Maxwell–Stefan surface diffusivities of components 1 and 2. $Đ_{12}$ represents the Maxwell–Stefan counter-sorption coefficient.

In analogy to the definition of the Knudsen diffusivity (Mason and Malinauskas, 1983) the Maxwell–Stefan micropore diffusivity is defined as

$$Đ \equiv \frac{Đ_{i,n+1}}{\theta_{n+1}}. \tag{3}$$

An alternative definition of the Maxwell–Stefan micropore diffusivity is adopted by Krishna (1990).

Mechanistically, the Maxwell–Stefan surface diffusivity $Đ_i$ may be related to the displacement of the adsorbed molecular species, λ, and the jump frequency, $\nu_i(\theta_t)$, which in general can be expected to be dependent on the total surface coverage (Reed and Ehrlich, 1981; Riekert, 1971; Zhdanov, 1985):

$$Đ = \frac{1}{z}\lambda^2 \nu_i(\theta_t). \tag{4}$$

In eq. (4) λ is the average jump distance; z is the number of nearest neighbour sites and $\nu_i(\theta_i)$ is the jump frequency of species i. If the jump frequency $\nu_i(\theta_i) = \nu_i(0)$ remains constant, independent of surface coverage, the Maxwell–Stefan surface diffusivity $Đ_i$ is also independent of surface coverage, i.e.

$$\nu_i(\theta_t) = \nu_i(0); \quad Đ_i = \frac{1}{z}\lambda^2 \nu_i(0). \tag{5}$$

The coefficients $Đ_{ij}$ express the adsorbate i and adsorbate j interactions. We can consider this coefficient as representing the facility for counter-exchange, i.e. at an adsorption site the sorbed species j is replaced by the species i. Krishna (1990) suggested the use of a Vignes (1996) relationship for determination of the counter-sorption diffusivity; alternative approaches are available in the literature (Yang *et al.*, 1991).

$$Đ_{ij} = [Đ_i(0)]^{\theta_i/(\theta_i+\theta_j)}[Đ_j(0)]^{\theta_j/(\theta_i+\theta_j)}. \tag{6}$$

Assuming equilibrium between the surface and the bulk fluid we have the following relationship for the surface chemical potential μ_i of species i:

$$\mu_i = \mu_i^0 + RT\ln(f_i) \tag{7}$$

where μ_i^0 is the chemical potential in the chosen standard state and f_i is the fugacity of species i in the bulk fluid mixture. For not too high system pressures the component partial pressures, p_i, can be used in place of the component fugacities, f_i, i.e. $f_i = p_i$. The surface chemical potential gradients may be expressed in terms of the gradients of the surface occupancies by introduction of the matrix of thermodynamic factors

$$\frac{\theta_i}{RT}\nabla\mu_i = \sum_{j=1}^{n}\Gamma_{ij}\nabla\theta_j, \quad \Gamma_{ij} \equiv \theta_i\frac{\partial \ln p_i}{\partial\theta_j}, \; i,j = 1,2,\ldots,n. \tag{8}$$

For the Langmuir isotherm

$$\theta_i = \frac{q_i^*}{q_{sat}} = \frac{b_i p_i}{1+\sum_{j=1}^{n} b_j p_j}, \quad b_i p_i = \frac{\theta_i}{1-\theta_t} \tag{9}$$

the elements of $[\Gamma]$ are

$$\Gamma_{ij} = \delta_{ij} + \frac{\theta_i}{(1-\theta_t)}, \quad i,j = 1,2,\ldots,n. \tag{10}$$

The surface concentration of component i, q_i^*, and the saturation concentration, q_{sat}, are commonly expressed in mol kg^{-1} of material (this is equivalent to expressing these in mmol g^{-1} as is commonly done in the literature) and the parameters b_i are usually expressed in units kPa^{-1}.

The surface fluxes $\mathbf{N}_i$ of the diffusing adsorbed species are defined as

$$\mathbf{N}_i = \rho\varepsilon q_{sat}\theta_i\mathbf{v}_i \tag{11}$$

where ρ is the particle density usually expressed in kg m^{-3}; ε is the porosity of the material. If the surface concentrations are expressed in mol kg^{-1}, the fluxes $\mathbf{N}_i$ are obtained in units of mol m^{-2} s^{-1}. The vacant sites can be considered to be stationary, so

$$\mathbf{v}_{n+1} = 0. \tag{12}$$

Combining eqs (1), (11) and (12) we obtain

$$-\frac{\theta_i}{RT}\nabla\mu_i = \sum_{\substack{j=1\\ j\neq i}}^{n}\frac{\theta_j\mathbf{N}_i - \theta_i\mathbf{N}_j}{\rho\varepsilon q_{sat}Đ_{ij}} + \frac{\mathbf{N}_i}{\rho\varepsilon q_{sat}Đ_i}; \quad i = 1,2,\ldots,n \tag{13}$$

which may be cast into n-dimensional matrix notation

$$-\rho\varepsilon q_{sat}[\Gamma](\nabla\theta) = [B](\mathbf{N}) \tag{14}$$

where the matrix $[B]$ has its elements which are given by

$$B_{ii} = \frac{1}{Đ_i} + \sum_{\substack{j=1\\ j\neq i}}^{n}\frac{\theta_j}{Đ_{ij}}, \quad i = 1,2,\ldots,n$$
$$B_{ij} = -\frac{\theta_i}{Đ_{ij}}, \quad i,j = 1,2,\ldots,n. \tag{15}$$

If we define a matrix of Fick surface diffusivities $[D]$ by

$$(\mathbf{N}) = -\rho\varepsilon q_{sat}[D](\nabla\theta) \tag{16}$$

we can obtain the following explicit expression for $[D]$:

$$[D] = [B]^{-1}[\Gamma]. \tag{17}$$

Equations (13)–(17) describe the complete generalized Maxwell–Stefan model for micropore diffusion. The major problem in the application of these equations is the determination of the counter-sorption diffusivities $Đ_{ij}$.

For single file diffusion mechanism, with no possibility of counter-exchange between the adsorbed species i and j, we can ignore the first right number of eq. (12). For the single file diffusion mechanism the above equations simplify to give the following expressions for the Fick surface diffusivity matrix $[D]$:

$$[D] = \begin{bmatrix} Đ_1 & 0 & 0 & 0 \\ 0 & Đ_2 & 0 & 0 \\ 0 & 0 & \ddots & 0 \\ 0 & 0 & 0 & Đ_n \end{bmatrix} [\Gamma]. \tag{18}$$

For single-component diffusion eqs (17) and (18) reduce to the scalar from

$$\mathbf{N}_1 = -\rho\varepsilon q_{sat} Đ_1 \Gamma \nabla\theta_1 \tag{19}$$

where the Fick surface diffusivity is

$$D_1 \equiv \frac{\mathbf{N}_1}{-\rho\varepsilon q_{sat}\nabla\theta_1} = Đ_1\Gamma. \tag{20}$$

For the Langmuir adsorption isotherm the thermodynamic factor Γ is

$$\Gamma = \frac{1}{1-\theta_1}. \tag{21}$$

Combining eqs (21) and (22) we obtain the following expression for the Fick micropore diffusivity:

$$D_1 = \frac{Đ_1}{(1-\theta_1)}. \tag{22}$$

For single file diffusion involving two components eqs (16)–(18) reduce to the two-dimensional form

$$(\mathbf{N}) = -\rho\varepsilon q_{sat} \begin{bmatrix} Đ_1 & 0 \\ 0 & Đ_2 \end{bmatrix} [\Gamma](\nabla\theta). \tag{23}$$

If we use the Langmuir isotherm to calculate $[\Gamma]$, we obtain

$$(\mathbf{N}) = -\rho\varepsilon q_{sat}[D](\nabla\theta),$$

$$[D] = \begin{bmatrix} Đ_1 & 0 \\ 0 & Đ_2 \end{bmatrix} \begin{bmatrix} 1-\theta_2 & \theta_1 \\ \theta_2 & 1-\theta_1 \end{bmatrix} \Big/ 1-\theta_1-\theta_2. \tag{24}$$

Expressions (24) are equivalent to the relations for the component effective diffusivities $D_{i,\mathrm{eff}}$ used by Habgood (1958) and Round *et al.* (1966). It must be emphasized that Habgood and Round derived the above expressions by *ad hoc* reasoning for the special case of two-component diffusion; there is no obvious method for generalizing their result to multicomponent mixtures. We have derived eq. (24) as a special case from the Maxwell–Stefan formulation. It is therefore possible for us to derive the correct general expression for the effective micropore diffusivities $D_{i,\mathrm{eff}}$ for a general n-component mixture.

Qureshi and Wei (1990) have also analysed the problem of diffusion of a binary mixture in a microporous solid. Krishna (1993a, b) has shown that the Qureshi-Wei model can be derived as a special case of the Maxwell–Stefan theory.

Simulations of transport within a single spherical particle

We first illustrate the use of the Maxwell–Stefan diffusion model by considering diffusion of a binary mixture inside a spherical microporous particle. The mixture consists of a fast-moving weakly adsorbed component (1) and a slow-moving strongly adsorbed component (2). The mathematical procedure used for calculation of the transient uptake profile within the spherical particle is the procedure outlined by Krishna (1990).

Firstly let us examine the (naïve) formulation based on the assumption of constant Fick matrix $[D]$, i.e.

$$[D] = \begin{bmatrix} Đ_1(0) & 0 & 0 & 0 \\ 0 & Đ_2(0) & 0 & 0 \\ 0 & 0 & \ddots & 0 \\ 0 & 0 & 0 & Đ_n(0) \end{bmatrix}. \tag{25}$$

Figure 2 compares the two models represented by eqs (24) and (25) for the estimation of the Fick $[D]$; these two models are seen to be *qualitatively* different. The constant Fick $[D]$ model predicts a monotonous approach to equilibrium for both components 1 and 2. The Maxwell–Stefan model based on eq. (24) predicts a maximum in the occupancy of the fast-moving component 1. The maximum in the surface occupancy can be explained as follows. Initially, we begin with a completely uncovered particle and this is exposed to a constant composition environment of components 1 and 2. The faster-moving component 1 will diffuse first inside the particle and occupy the vacant sites. When the slower-moving component 2 enters the particle it will "dislodge" component 1 because of the higher adsorption strength of component 2. The final, equilibrium, surface occupancies will reflect the differences in the adsorption strengths. In the initial stages it is possible to obtain higher occupancies of the faster-moving component 1 because of differences in mobilities inside the particle.

In Fig. 3 we test the importance of counter-sorption in the Maxwell–Stefan formulation. The complete Maxwell–Stefan formulation including counter-sorption, eqs (6), (15) and (16), is compared with the limiting case of single file diffusion, eq. (24). The simulation results in Fig. 2 show that inclusion of counter-sorption does not change the essential features of the transient uptake, namely the existence of a maximum in the occupancy of component 1. The differences in the simulation results are minor. In the following

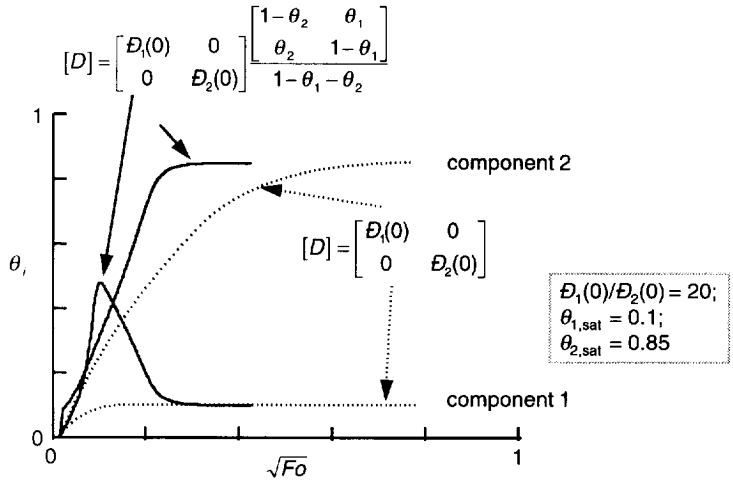

Fig. 2. Transient uptake profiles of a binary mixture inside a single spherical particle. The single file diffusion model is compared with a model in which the Fick surface diffusivity is assumed to be coverage independent. The Fourier number is defined as $F_0 = 4Đ_1(0)\, t/d_p^2$.

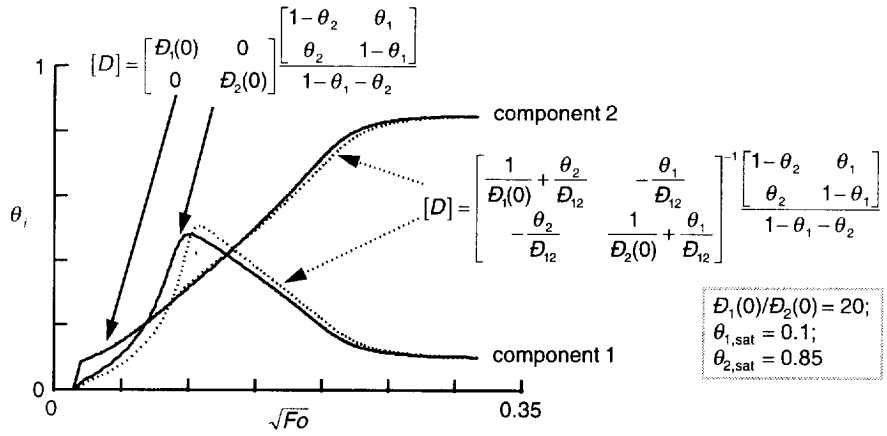

Fig. 3. Transient uptake profiles of a binary mixture inside a single spherical particle. The single file diffusion model is compared with the complete Maxwell–Stefan model including counter-sorption, with $Đ_{12}$ given by eq. (6). The Fourier number is defined as $F_0 = 4Đ_1(0)\, t/d_p^2$.

treatment we, therefore, adopt the single file diffusion model (18).

If the single-component diffusivities $Đ_i$ are determined experimentally, the Maxwell–Stefan theory provides a method for predicting the behaviour of multicomponent diffusion behaviour with the help of relations (16) and (17). In general we will require multicomponent adsorption equilibrium data for calculation of the elements of the matrix of thermodynamic factors $[\Gamma]$. We aim to validate the use of Maxwell–Stefan theory for predicting the mixture behaviour. Further we aim to show that the constant Fick $[Đ]$ model is not of adequate accuracy.

EXPERIMENTAL

A schematic diagram of the experimental set-up is shown in Fig. 4. The apparatus used for measuring the step response consists of a gas feed selection part, a packed column section (with furnace) and a gas analysis section. The gas selection section consists of a four-way switch valve which is operated pneumatically. Using the switch valve we can choose between two different gas flows, one is the purge flow, most of the time helium, and the other one the mixture flow with the adsorbable components. A constant flow rate for all the experiments was established by use of two mass-flow controllers (HI-TEC series F100/200). Prior to every experiment the flow controllers were calibrated for the different gas mixtures. After the flow controller and before the column two pressure transducers and equalizers (from Ametek) were placed. The column itself is placed in a furnace, to provide (near) isothermal conditions. The temperature in the furnace was set by a West 2073 self-tuning controller. The stainless steel column was packed with spherical microporous carbon adsorbents. Two different adsorption columns have been used throughout the experimental program.

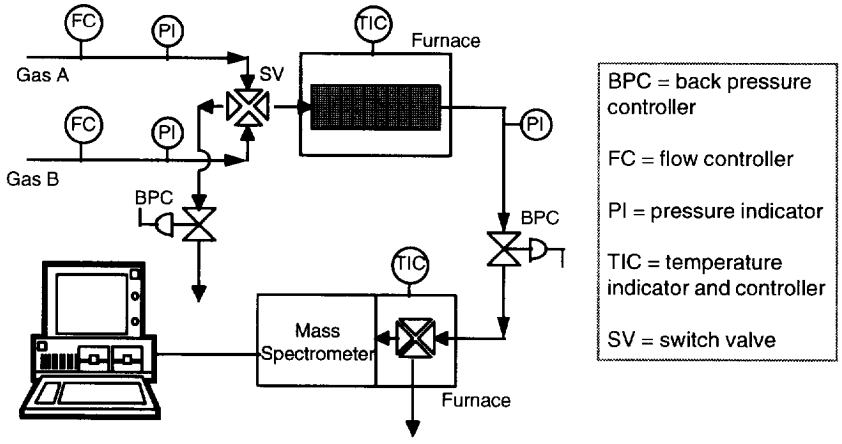

Fig. 4. Experimental set-up used for breakthrough experiments.

In this study two almost identical columns have been used. The first column was packed with a microporous activated carbon (MAC), obtained from Kureha, Osaka (Japan). The other column was packed with a carbon molecular sieve (CMS) from Takeda, Tokyo (Japan). The specifications of the adsorption columns, the experimental conditions, and the properties of the adsorbents are given in Tables 1 and 2.

Between the column and the mass spectrometer a pressure transducer and a back pressure controller (HI-TEC series P500/600/700) are placed. The effluent concentration profiles are analysed continuously with a Leybold-Heraeus quadrupole mass spectrometer (Quadruvac Q200). Gas was introduced into the mass spectrometer via a heated relief valve (Balzers UDV 135) and a capillary, kept at a temperature of 383 K.

Table 1. Column specifications and experimental conditions for the two adsorption columns

Column length, L (m)	0.3
Column internal diameter (m)	0.01
Porosity of bed, ε_b (−)	
Kureha microporous activated carbon	0.4
Takeda carbon molecular sieve	0.43
Temperature, T (K)	315, 345 or 375
System pressure, p (kPa)	200
Gas velocity at inlet, u_0 (m s^{-1})	0.003 or 0.01

The mass spectrometer is connected to a turbomolecular pump (Balzers TSU 180 H).

The experimental set-up and the data processing are fully controlled by computer; see Fig. 4.

Characterization of the adsorbents

As adsorbent two microporous carbons have been used. First a series of experiments have been performed with Kureha spherical BAC-MQ [bead activated carbon (BAC), Kureha Chemical Co., Osaka, Japan]; this is a microporous activated carbon (MAC). This adsorbent is referred to as Kureha MAC. The particles are of uniform size and spherical, with a particle diameter $d_p = 460$ μm. A second series of experiments have been performed with a 5A carbon molecular sieve from Takeda (Shirasagi CMS 5A, lot no. M23MM2, Takeda Chemical Industries Ltd, Tokyo, Japan). This adsorbent is referred to as Takeda CMS.

The structural properties of the adsorbent particles were determined by a Sorptomatic 1800 for the nitrogen adsorption (BET characterization) and a Porosimeter 4000 for mercury porosimetry, both from Carlo Erba Strumentazione. The characterization of the microporous adsorbent particles is summarized in Table 2. The pore size distribution is depicted in Fig. 5. The pore diameter for the Kureha MAC adsorbent is smaller than 2 nm and therefore lies completely in the microporous range. The average pore

Table 2. Characterization of the Kureha microporous activated carbon (MAC) and the Takada carbon molecular sieve (CMS)

	Kureha MAC	Takeda CMS
Average particle radius, (d_p/2) (μm)	230	180
Internal porosity (−)	0.64	0.54
Skelet density, ρ (kg m^{-3})	2100	2000
Apparent surface area, S_A (m^2 g^{-1})	1513	617
Average pore diameter (nm)†	0.52	0.45
Pore volume, V_p (cm^3 g^{-1})	0.78	0.28

†Slit model: pore diameter = V_p/S_A.

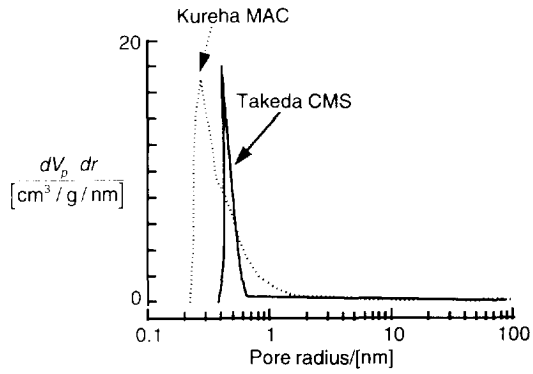

Fig. 5. Pore size distributions for Takeda carbon molecular sieve and Kureha microporous activated carbon.

diameter is about 1 nm. Furthermore, 80% of the total internal volume lies in the range with a pore diameter smaller than 1.2 nm. The carbon molecular sieve from Takeda has an average pore diameter of 0.5 nm.

Experimental procedure

Prior to every experiment the adsorption column was regenerated for several hours at a temperature of 392 K and purged with a helium flow. After this the packed bed was brought to the experimental temperature and flow rates. From the experimental set-up shown in Fig. 4 it is clear that response to two different gaseous flows can be studied. In general, one flow was the helium purge. At time $t = 0$, a step of an adsorbing gas (single-component or multicomponent) was introduced into the column.

Three different types of experiments have been performed.

(*a*) *Single-component adsorption and desorption experiments.* In the adsorption experiments a step input of a single-component gas was introduced into the column. The desorption experiments were performed by purging the column, which is in equilibrium with the adsorbed gas, with helium. In both adsorption and desorption experiments the effluent concentrations were monitored continuously with the mass spectrometer. The inlet concentrations of the adsorbing gas were varied by mixing the pure components with a known amount of helium.

(*b*) *Co-sorption of binary and ternary mixtures.* A mixture with a specified composition was prepared and introduced into the column as a step input. The effluent composition was monitored continuously as a function of time.

(*c*) *Counter-sorption experiments.* In these experiments the column is first equilibrated with one adsorbing species. Then this component is displaced by introduction of a second species and the column response monitored continuously by means of the mass spectrometer.

The gaseous components used in the above experiments were CO_2, N_2, CH_4, C_3H_6 and C_3H_8.

Determination of the adsorption isotherms

For the simulation of the experiments we also need the adsorption isotherms. These isotherms were measured for the single- and multi-component systems with a Sorptomatic 1800, operated by a Milestone 200 program. For single-component isotherms, the constants b and q_{sat} in the Langmuir relation

$$q^* = q_{sat}\frac{bp}{1+bp} \tag{26}$$

are listed in Table 1 for the various species. These single-component adsorption data can be used for prediction of multicomponent isotherms using the extended Langmuir isotherm

$$q_i^* = q_{sat}\frac{b_i p_i}{1 + b_1p_1 + b_2p_2 + \cdots + b_np_n}. \tag{27}$$

NUMERICAL MODELLING OF BREAKTHROUGH EXPERIMENTS

For the simulation of the breakthrough experiments we need to set up a mathematical description of the column dynamics. The subject of modelling of the dynamics of adsorption columns is extensively discussed in the literature (Kärger and Ruthven, 1992; Ruthven, 1984; Ruthven *et al.*, 1994; Yang, 1987). A brief summary of the model formulation, and numerical solution is given below.

The model

The axially dispersed plug flow model is adopted. The fluid-phase mass balance for component i is given by

$$\frac{\partial c_i}{\partial t} = E\frac{\partial^2 c_i}{\partial z^2} - \frac{\partial (uc_i)}{\partial z} - \left(\frac{1-\varepsilon_b}{\varepsilon_b}\right)\rho\frac{\partial \bar{q}_i}{\partial t} \tag{28}$$

where E is the axial dispersion coefficient; u is the fluid (gas)-phase velocity, which in general varies along the packed bed; z is the axial distance coordinate; ε_b is the porosity of the bed; ρ is the density of the solid adsorbents; c_i is the molar concentration in the gas phase.

The average concentration within the spherical particle is

$$\bar{q}_i = \frac{3}{(d_p/2)^3}\int_0^{d_p/2} q_i r^2\,\mathrm{d}r. \tag{29}$$

In the numerical simulations to be presented later the packed bed is assumed to operate isothermally, the pressure drop is considered to be negligible and the ideal gas law has been assumed.

Models for micropore diffusion

As the focus in this paper is on the description of the intraparticle micropore diffusion, we performed the simulations using three different models as discussed below.

(1) *Linear driving force (LDF) model with constant diffusivities*

$$\frac{\partial \bar{q}_i}{\partial t} = 15 \times \frac{4D_i}{d_p^2}(q_i^* - \bar{q}_i). \tag{30}$$

In this case the diffusion resistance is assumed to be restricted to a thin spherical layer around the particle. This linear driving force model is discussed thoroughly in standard texts (Kärger and Ruthven, 1992; Ruthven, 1984; Ruthven *et al.*, 1994; Yang, 1987). The diffusivities are taken equal to the Maxwell–Stefan single-component micropore diffusivities at zero coverage, i.e. $D_i = Đ_i(0)$.

(2) *Solid diffusion model with a concentration-independent diagonal Fick matrix of diffusivities*

$$\frac{\partial q_i}{\partial t} = D_i\left(\frac{\partial^2 q_i}{\partial r^2} + \frac{2}{r}\frac{\partial q_i}{\partial r}\right). \tag{31}$$

Here the unsteady-state diffusion process within the particle is taken into account by the model used to describe the diffusion process assuming a constant matrix of Fick diffusivities. Further the matrix of diffusivities $[D]$ is assumed to be diagonal and the diagonal elements are set equal to the Maxwell–Stefan diffusivities at zero coverage, i.e. $D_i = Đ(0)$.

(3) *Solid diffusion model with a concentration-dependent Fick matrix of diffusivities*

$$\frac{\partial q_i}{\partial r} = \frac{1}{r}\frac{\partial}{\partial r}\left(r^2 \sum_{k=1}^{n} D_{ik}\frac{\partial q_k}{\partial r}\right) \tag{32}$$

where the matrix of Fick diffusivities is dependent on the surface coverages and is given by eq. (17).

Axial dispersion and external mass transfer resistances

The axial dispersion coefficient E was estimated from the correlations of Wakao and co-workers (Wakao *et al.*, 1978; Wakao and Funazkri, 1979):

$$E = \frac{0.23D_{12}^M}{\varepsilon_b} + ud_p/2. \tag{33}$$

Further, in the simulations to be presented later, the external mass transfer resistance was accounted for by using the correlation

$$Sh = \frac{k_f d_p}{D_{12}^M} = 2 + 1.1(Re)^{0.6}(Sc)^{1/3}. \tag{34}$$

However, this mass transfer resistance was not found to be significant for the conditions of the experiments.

The method of lines (Schiesser, 1991) was used to solve the set of partial differential equations describing the column dynamics. In order to test our numerical procedure outlined above we attempted to simulate one of the published breakthrough simulations reported by Farooq and Ruthven (1991a) for O_2/N_2 in a packed bed of carbon molecular sieves using the LDF model with constant Fick matrix $[D]$. The results of our own LDF simulations using the method of lines coincide extremely well with the results of Farooq and Ruthven (1991a) who use orthogonal collocation.

SINGLE-COMPONENT BREAKTHROUGH EXPERIMENTS

Influence of feed composition on breakthrough

Figure 6 shows the adsorption and desorption experiments with varying proportions of CH_4/He in the feed at a constant inlet pressure and temperature using Kureha MAC. Figure 7 shows adsorption experiments with varying feed compositions of CO_2/He using Takeda CMS. These experiments were fitted with the Maxwell–Stefan single file diffusion model to obtain the Maxwell–Stefan diffusivity $Đ_i$. The $(4Đ_i/d_p^2)$ values thus fitted are plotted in Fig. 8 against the saturation concentration θ_{sat} calculated as follows:

$$\theta_{sat} = \frac{bp}{1 + bp} \tag{35}$$

where p is the partial pressure of the sorbed species in the gas phase at the inlet to the packed bed. As seen in Fig. 8 the $Đ_i$ are independent of the equilibrium occupancy θ_{sat}. This means that the single file diffusion model with constant values of the Maxwell–Stefan diffusivity reflects the diffusion processes very well. Table 4 lists the values of $[4Đ_i(0)/d_p^2]$ obtained from the set of single-component sorption experiments performed. The results of simulations of breakthrough experiments with pure gases are shown in Fig. 9. Even in this extreme situation the breakthrough experiments can be predicted with the same values of

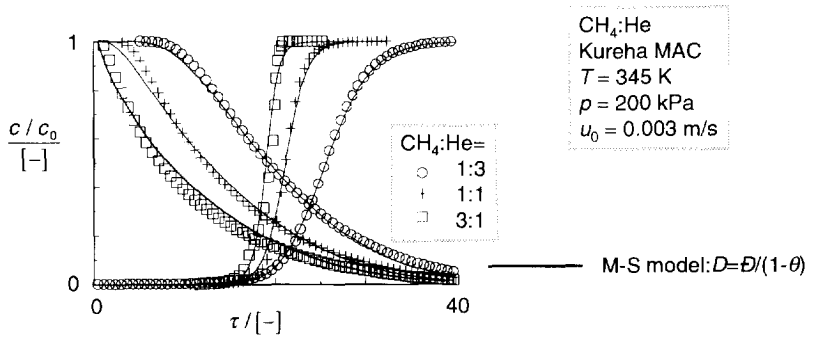

Fig. 6. One-component breakthrough curve for CH_4/He in various proportions on Kureha microporous activated carbon adsorbent particle. The markers are experimental results and the solid lines are numerical fits with the single file diffusion model taking the Maxwell–Stefan diffusion coefficient to be constant and the Fick diffusivity $D = Đ/(1 - \theta)$. The variation of the gas velocity u along the length of the column is accounted for.

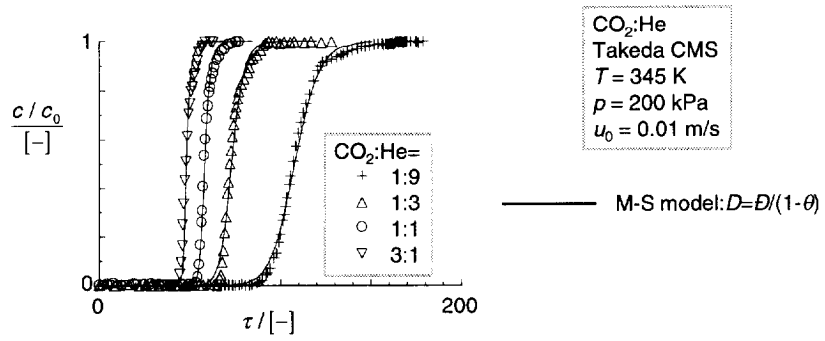

Fig. 7. One-component breakthrough curve for CO_2/He in various proportions on Takeda CMS adsorbent particle. The markers are experimental results and the solid lines are numerical fits with the single file diffusion model taking the Maxwell–Stefan diffusion coefficient to be constant and the Fick diffusivity $D = Đ/(1 - \theta)$. The variation of the gas velocity u along the length of the column is accounted for.

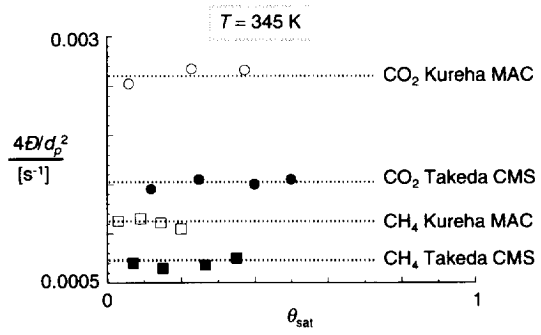

Fig. 8. The Maxwell–Stefan single-component micropore diffusivities for methane and carbon dioxide in Kureha microporous activated carbon and in Takeda carbon molecular sieve particles. These diffusivities are obtained from breakthrough experiments with varying feed compositions. The x-axis represents the saturation coverage of the particles calculated on the basis of equilibrium with the inlet feed composition, temperature and pressure.

$[4Đ_i(0)/d_p^2]$ as obtained with dilute systems (i.e. zero coverage), confirming the constancy of the Maxwell–Stefan diffusivity values.

Influence of temperature

Both Kureha MAC and Takeda CMS breakthrough experiments with dilute CH_4/He and dilute CO_2/He were carried out at three different temperatures. The Arrhenius plot of the fitted values of the $[4Đ_i(0)/d_p^2]$ is shown in Fig. 10. The Arrhenius dependence of the Maxwell–Stefan diffusivity is evident and this confirms that micropore diffusion is an activated process; see Fig. 1. The activation energy for diffusion of CH_4 on Kureha MAC, for example, is found to be 5.6 kJ mol^{-1}, slightly smaller than the corresponding heat of adsorption.

Influence of varying feed velocity

We have also investigated the influence of varying the inlet feed velocity. Breakthrough experiments with CH_4/He on Takeda CMS are shown in Fig. 11 at two different values of u_0 = 0.003 and 0.01 m s^{-1}. Increasing the inlet feed gas velocity increases the value of the Peclet number, $Pe = u_0 L/E$, evaluated using eq. (32). Both sets of experiments could be simulated using the same values of the Maxwell–Stefan diffusivity $Đ_i$ (0), as seen in Fig. 11. The results of the simulations confirm, indirectly, that the intraparticle micropore

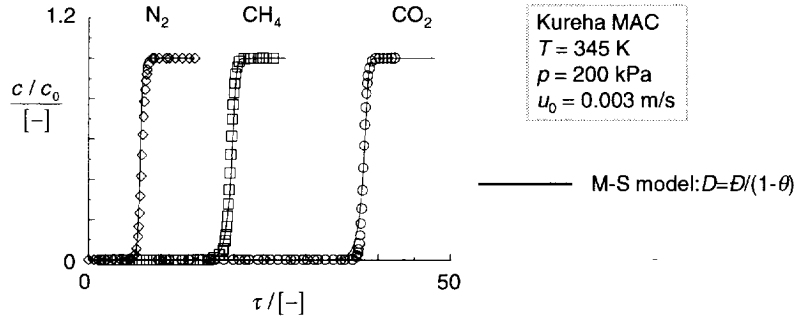

Fig. 9. One-component breakthrough curve for pure gases N_2, CH_4 and CO_2 on Kureha microporous activated carbon adsorbent particles. The markers are experimental results and the solid lines are numerical fits with the single file diffusion model taking the Maxwell–Stefan diffusion coefficient to be constant and the Fick diffusivity $D = Đ/(1 - \theta)$. The variation of the gas velocity u along the length of the column is accounted for.

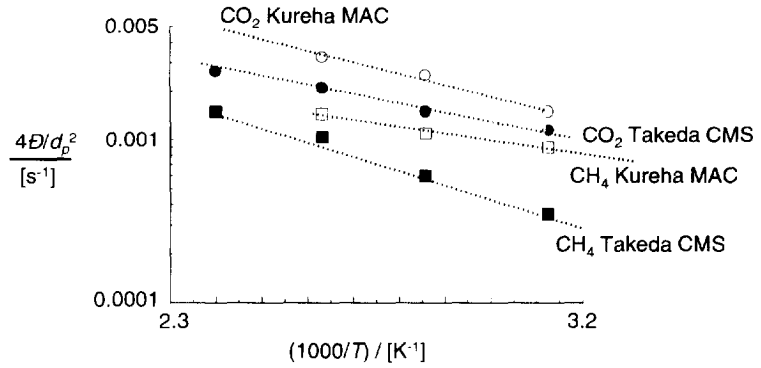

Fig. 10. The Maxwell–Stefan single-component micropore diffusivities for methane and carbon dioxide in Kureha microporous activated carbon and in Takeda carbon molecular sieve particles. The data confirm the Arrhenius dependence of $Đ$ on temperature T.

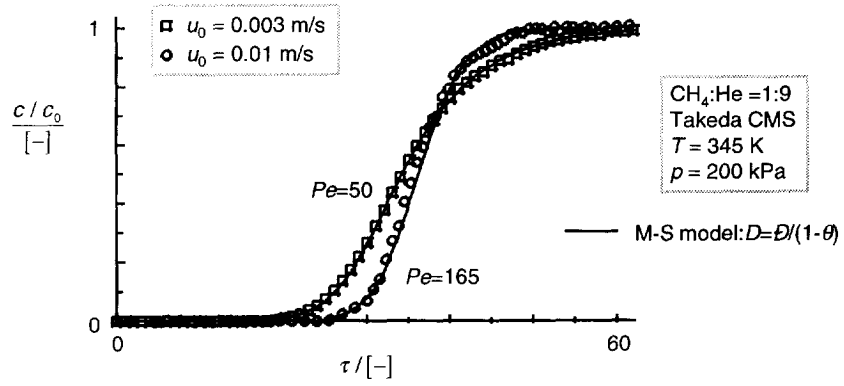

Fig. 11. The influence of varying feed velocity on the breakthrough of methane–helium mixture on Takeda CMS.

diffusion process is the controlling diffusional resistance.

MULTICOMPONENT BREAKTHROUGH EXPERIMENTS

Co-sorption, de-sorption, counter-sorption and displacement experiments with methane/carbon dioxide mixtures

Figure 12 shows the results of co-sorption experiments with a mixture of CH_4 and CO_2 using He as inert gas using a packed bed of Kureha MAC as adsorbent. The experiments have been simulated with the single-component Maxwell–Stefan diffusivity values $Đ_i(0)$ reported in Table 4. The equilibrium was predicted using the extended Langmuir isotherm, eq. (12) with the parameter values as listed in Table 3.

In Fig. 12 three different model predictions are compared:

(i) the LDF model with concentration-independent diffusivities, $Đ_i(0)$,

(ii) a solid diffusion model with constant diagonal matrix of Fick diffusivities, $D_i = Đ_i(0)$, and

(iii) the Maxwell–Stefan single file diffusion model for micropore diffusion.

The roll-up phenomenon observed experimentally in Fig. 12 is primarily caused by the differences in the adsorption strengths of methane and carbon dioxide. Carbon dioxide is more strongly adsorbed and is retained within the pores. This results in a higher concentration in the bulk gas phase, which in the initial stages of breakthrough can be higher than the inlet feed concentration. We see that predictions of the Maxwell–Stefan single file diffusion model are clearly superior to those of the other two models. The simple LDF model does a surprisingly good job of predicting the roll-up of methane. The constant Fick [D] model (ii) is not very successful in predicting the co-sorption behaviour; this model predicts only a 3% overshoot in the breakthrough of methane. Further, these simulations with constant Fick [D] model (ii) appear to be very sensitive to the values of the diffusivities.

We conclude from Fig. 12 that the Maxwell–Stefan single file diffusion model is superior to the other two models. In the rest of this paper only the simulations of this Maxwell–Stefan single file diffusion model will be presented.

Figure 13 shows *ad*sorption and *de*sorption of the mixture of CH_4 and CO_2. Both these processes can be

Table 3. The Langmuir isotherm parameters for single components on Kureha MAC and Takeda CMS

System	T (K)	b (kPa^{-1})	q_{sat} (mol kg^{-1})
CO_2/Takada CMS	273	0.036	4.09
CH_4/Kureha MAC	315	0.0033	2.05
CO_2/Kureha MAC	315	0.0057	3.01
CH_4/Takeda CMS	315	0.0071	1.49
CO_2/Takeda CMS	315	0.012	2.38
N_2/Kureha MAC	345	0.003	0.38
CH_4/Kureha MAC	345	0.0027	1.8
CO_2/Kureha MAC	345	0.003	2.4
CH_4/Takeda CMS	345	0.0036	1.35
CO_2/Takeda CMS	345	0.0066	2
C_3H_6/Kureha MAC	375	0.02	2.3
C_3H_8/Kureha MAC	375	0.021	2.3
C_3H_6/Takeda CMS	375	0.082	1.6
C_3H_8/Takeda CMS	375	0.013	1.9
CH_4/Kureha MAC	375	0.0024	0.71
CO_2/Kureha MAC	375	0.0019	2.3
CH_4/Takeda CMS	375	0.0046	0.45
CO_2/Takeda CMS	375	0.0055	1.47
CH_4/Takeda CMS	415	0.004	0.35
CO_2/Takeda CMS	415	0.0045	0.37

Table 4. Single-component Maxwell–Stefan diffusivity values

	T (K)	$[4Đ_i(0)/d_p^2]$ (s^{-1})
N_2/Kureha MAC	345	0.006
CH_4/Kureha MAC	345	0.0026
CO_2/Kureha MAC	345	0.0011
CH_4/Takeda CMS	345	0.0016
CO_2/Takeda CMS	345	0.0007
C_3H_8/Kureha MAC	375	0.0015
C_3H_8/Kureha MAC	375	0.0007
C_3H_6/Takeda CMS	375	0.0004
C_3H_8/Takeda CMS	375	0.0001

described with the *same* values of the Maxwell–Stefan diffusivities $Đ_i(0)$.

Figure 14 shows the results of counter-diffusion experiments. In one set of experiments a column operating under equilibrium breakthrough with pure CH_4 is suddenly switched to a feed of CO_2. In another experiment a column operating under equilibrium breakthrough with pure CO_2 is suddenly switched to a feed of CH_4. Both sets of experiments are simulated successfully with the Maxwell–Stefan diffusion model.

In Fig. 15 the column packed with Kureha MAC operating at equilibrium with a mixture of 25%

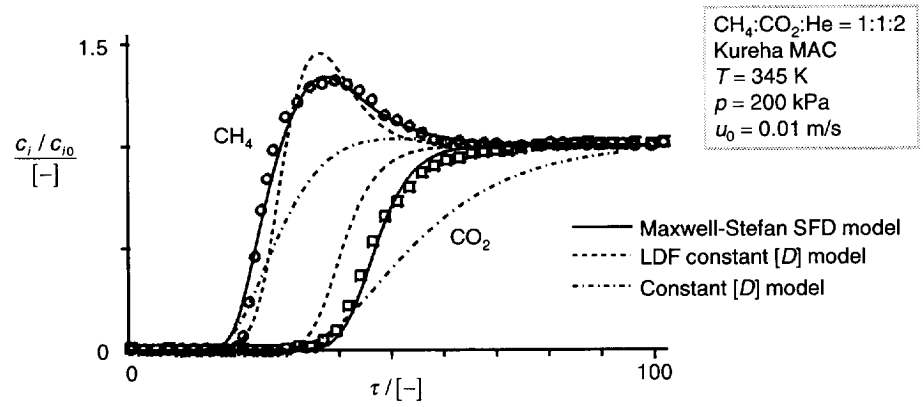

Fig. 12. Breakthrough curves for the system CH_4/CO_2/He in the ratio of 1 : 1 : 2 with Kureha microporous carbon adsorbent particles. The effluent concentration is plotted on the y-axis and this is normalized with respect to the inlet concentration. On the x-axis is plotted the dimensionless time, $\tau = tu_0/L$. The markers are experimental results and the solid lines are numerical fits with the single file diffusion model taking the Maxwell–Stefan diffusion coefficients $Đ_1$ and $Đ_2$ to be constant. Also shown are the simulations with the constant $[Đ]$ model and the LDF model. The variation of the gas velocity u along the length of the column is accounted for.

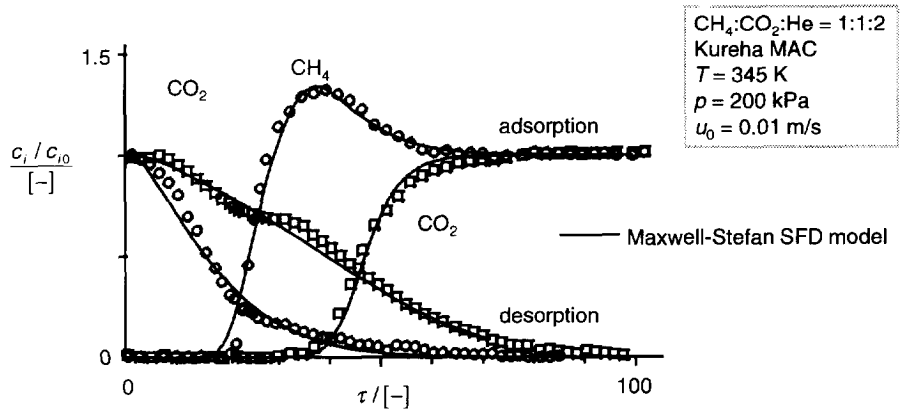

Fig. 13. Adsorption and desorption breakthrough curves for the system CH_4/CO_2/He in the ratio of 1 : 1 : 2 with Kureha microporous carbon adsorbent particles. The effluent concentration is plotted on the y-axis and this is normalized with respect to the inlet concentration. On the x-axis is plotted the dimensionless time, $\tau = tu_0/L$. The markers are experimental results and the solid lines are numerical fits with the single file diffusion model taking the Maxwell–Stefan diffusion coefficients $Đ_1$ and $Đ_2$ to be constant. The variation of the gas velocity u along the length of the column is accounted for.

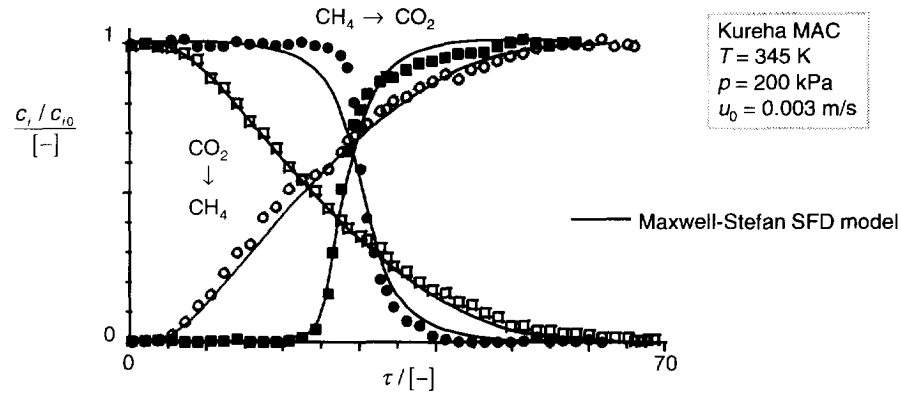

Fig. 14. Breakthrough curves for counter-diffusion in the system CH_4/CO_2 with the Kureha microporous carbon adsorbent particles. The effluent concentration is plotted on the y-axis and this is normalized with respect to the inlet concentration. On the x-axis is plotted the dimensionless time, $\tau = tu_0/L$. The markers are experimental results and the solid lines are numerical fits with the single file diffusion model taking the Maxwell–Stefan diffusion coefficients $Đ_1$ and $Đ_2$ to be constant. The variation of the gas velocity u along the length of the column is accounted for.

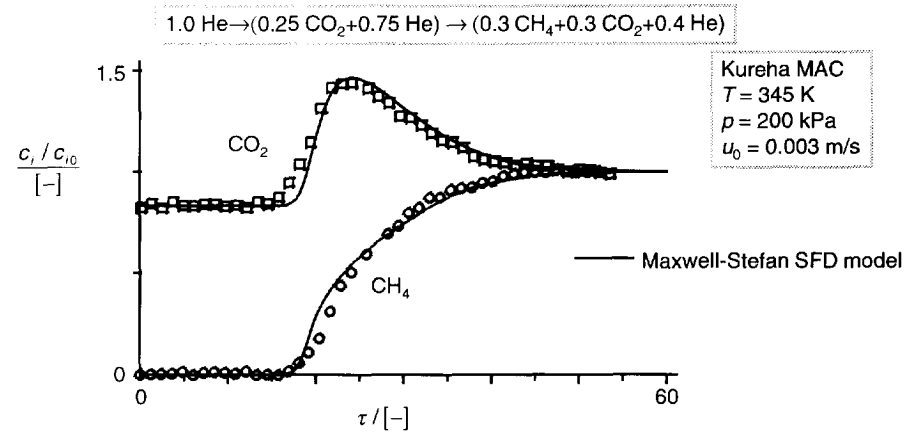

Fig. 15. Breakthrough curves for a step change from time $t = 0$ of a gas mixture (0.25 CO_2 + 0.75 **He**) with the mixture (0.3 CO_2 + 0.3 CH_4 + 0.4 He). Kureha microporous carbon is used as adsorbent. The effluent concentration is plotted on the y-axis and this is normalized with respect to the inlet concentration. On the x-axis is plotted the dimensionless time, $\tau = tu_0/L$. The markers are experimental results and the solid lines are numerical fits with the single file diffusion model taking the Maxwell–Stefan diffusion coefficients $Đ_1$ and $Đ_2$ to be constant. The variation of the gas velocity u along the length of the column is accounted for.

CO_2/75% He is suddenly switched to a feed of 30% CO_2/30% CH_4/40% He. This switch results in a roll-up for CO_2 and the whole column dynamics can be simulated well by the Maxwell–Stefan single file diffusion model.

Influence of varying binary feed composition on co-sorption behaviour

Figure 16 studies the influence of varying the feed composition of the roll-up behaviour of a mixture of CH_4 and CO_2 using Kureha MAC adsorbent. There is a pronounced influence of varying feed composition of CH_4 and CO_2 on the roll-up of methane. With increasing composition of the less strongly adsorbed CH_4 the roll-up of this component becomes progressively less pronounced. The concentration effect can be simulated well with the Maxwell–Stefan model.

Influence of varying gas velocity of breakthrough behaviour

Due to the adsorption process the gas velocity will be altered. This phenomenon was earlier encountered in the simulation of oxygen–nitrogen breakthrough on carbon molecular sieve; see Fig. 11. In Fig. 17 we present the experimental breakthrough results with CH_4 and CO_2 on Takeda CMS. Simulations were carried out with the Maxwell–Stefan single file diffusion model with two different approaches: (i) taking the variation of the gas velocity into account, as is done normally in all the simulations reported thus far,

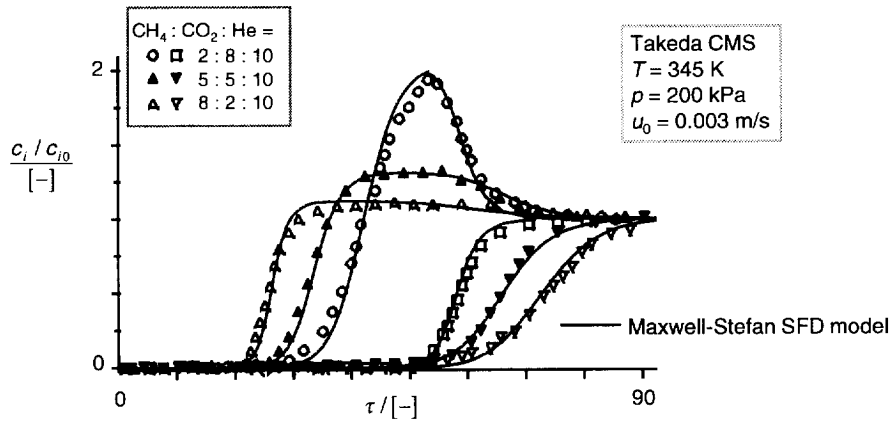

Fig. 16. Breakthrough curves for binary mixtures of CH_4 and CO_2 with He as inert gas. Kureha microporous carbon is used as absorbent. The effluent concentration is plotted on the y-axis and this is normalized with respect to the inlet concentration. On the x-axis is plotted the dimensionless time, $\tau = tu_0/L$. The markers are experimental results and the solid lines are numerical fits with the single file diffusion model taking the Maxwell–Stefan diffusion coefficients $Đ_1$ and $Đ_2$ to be constant. The variation of the gas velocity u along the length of the column is accounted for.

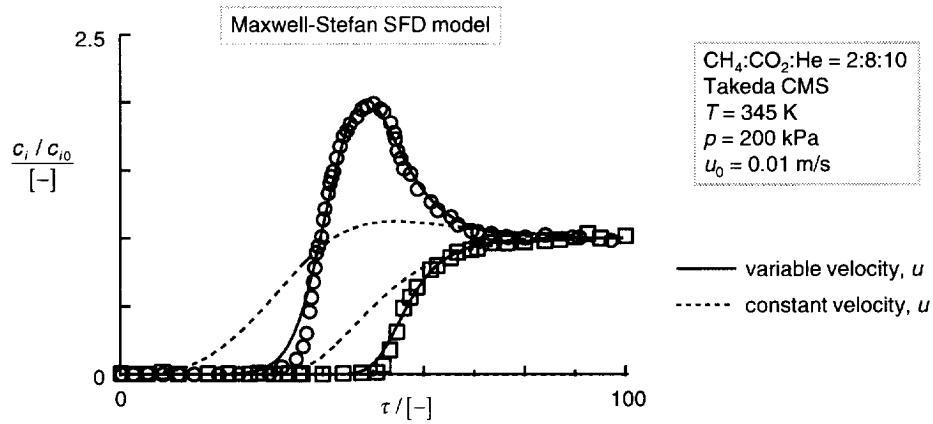

Fig. 17. Breakthrough curves for binary mixtures of CH_4 and CO_2 with He as inert gas. Kureha microporous carbon is used as adsorbent. The effluent concentration is plotted on the y-axis and this is normalized with respect to the inlet concentration. On the x-axis is plotted the dimensionless time, $\tau = tu_0/L$. The markers are experimental results and the solid lines are numerical fits with the single file diffusion model taking the Maxwell–Stefan diffusion coefficients $Đ_1$ and $Đ_2$ to be constant. Two sets of simulations have been performed: (i) allowing variation of the gas velocity u along the length of the column due to finite adsorption, and (ii) ignoring the velocity variation and taking $u = u_0$.

and (ii) assuming constant gas velocity, i.e. taking $u = u_0$. It can be observed that the assumption of constant gas velocity leads to extremely poor agreement with the experiments; in particular the roll-up of methane is not observed in this case.

Breakthrough of ternary mixture

A stringent test of the predictive capability of the Maxwell–Stefan single file model is to simulate the breakthrough of a ternary mixture. Figure 18 shows the results obtained in the packed bed of Kureha MAC with the mixture N_2, CH_4 and CO_2. The single-component diffusivity values in Table 4, along with the single-component equilibrium constants listed in Table 3, were used in performing the simulations. The extended Langmuir isotherm was used to predict the ternary adsorption equilibrium. The simulation results are quite good, especially when we consider that no multicomponent diffusion or equilibrium data have been used in the data inputs. The breakthrough roll-up of nitrogen is quite sensitive to the equilibrium parameters and is not predicted as well as the breakthrough of the other, more strongly adsorbed components.

Breakthrough of propane/propene mixture

On Kureha microporous activated carbon, propane and propene have almost similar adsorption strengths; see Table 3. Breakthrough experiments with the binary mixture of propane and propene in the presence of inert gas He show that propene exhibits a roll-up effect; see Fig. 19. There is a finite

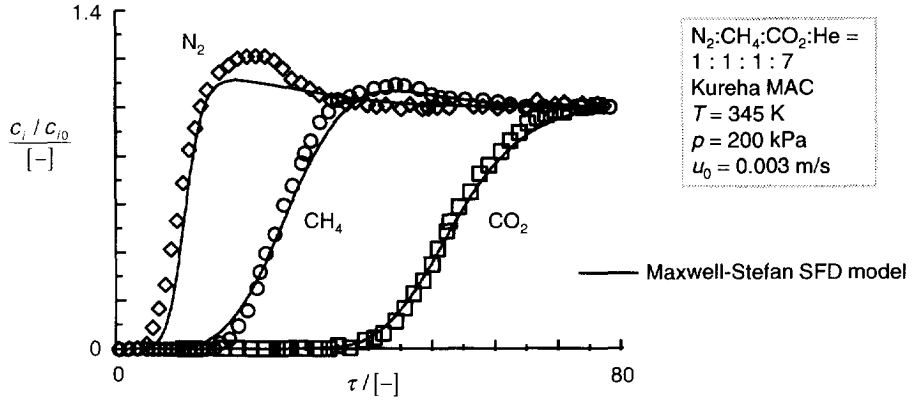

Fig. 18. Breakthrough curves for a ternary mixture of N_2, CH_4 and CO_2 with He as inert gas. Kureha microporous carbon is used as adsorbent. The effluent concentration is plotted on the y-axis and this is normalized with respect to the inlet concentration. On the x-axis is plotted the dimensionless time, $\tau = tu_0/L$. The markers are experimental results and the solid lines are numerical fits with the single file diffusion model taking the Maxwell–Stefan diffusion coefficients $Đ_1$, $Đ_2$ and $Đ_3$ to be constant. The variation of the gas velocity u along the length of the column is accounted for.

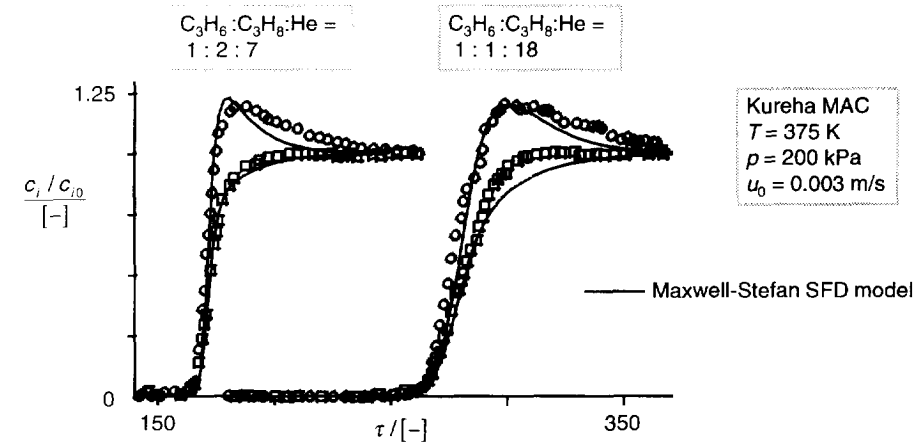

Fig. 19. Breakthrough curves for the dilute systems C_3H_6/C_3H_8 with He as inert gas. Two composition sets have been studied with Kureha microporous activated carbon adsorbent particles. The markers are experimental results and the solid lines are numerical fits with the single file diffusion model taking the Maxwell–Stefan diffusion coefficients $Đ_1$ and $Đ_2$ to be constant. The variation of the gas velocity u along the length of the column is accounted for.

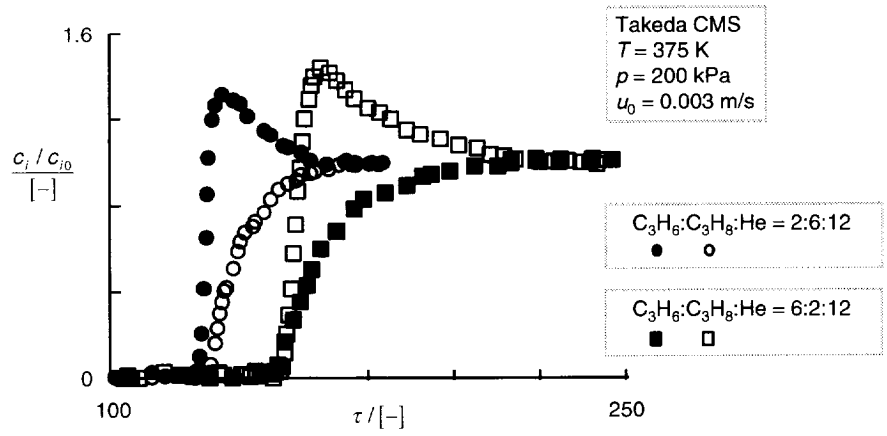

Fig. 20. Breakthrough curves for the system C_3H_6/C_3H_8 with He as inert gas. Two composition sets have been studied with Takeda CMS as adsorbent.

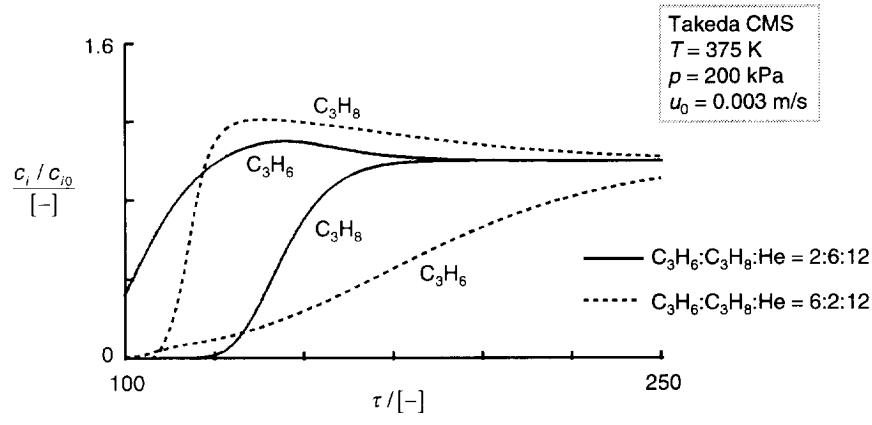

Fig. 21. Simulations of breakthrough curves for the system C_3H_6/C_3H_8 with He as inert gas. Two composition sets have been studied with Takeda CMS as adsorbent. The simulations were performed using the single file Maxwell–Stefan diffusion model. For the simulations presented above the extended Langmuir isotherm has to be further modified using "discount factors" of Gu *et al.* (1991).

difference in the values of the Maxwell–Stefan diffusivities for these two components $(4\mathcal{D}_{\text{propane}}/d_p^2) = 0.0015\ \text{s}^{-1}$; $(4\mathcal{D}_{\text{propane}}/d_p^2) = 0.0007\ \text{s}^{-1}$. When the concentration of propene is increased in the feed mixture the roll-up phenomenon for this component becomes less pronounced, in conformity with the results reported above for mixtures of CH_4 and CO_2. Simulations using the single-component diffusivity and equilibrium data, along with the extended Langmuir relations (27), are not as good as the simulation results reported in the foregoing probably due to poorer fits of the adsorption isotherms.

For Takeda CMS, breakthrough experiments with varying feed composition show the phenomenon of reversal of roll-up; see Fig. 20. Attempts to simulate this phenomenon by means of the single-component diffusivity data (Table 4) and single-component isotherm parameters (Table 3) were not successful due to the fact that the binary adsorption equilibrium is not properly described by the extended Langmuir isotherm. If the extended Langmuir isotherm is further modified to include a "discount" factor $\xi_{12} = q_{1,\text{sat}}/q_{2,\text{sat}}$ as suggested by Gu *et al.* (1991)

$$\theta_1^* = \frac{b_1 p_1}{1 + b_1 p_1 + b_2 p_2 + (1 - \xi_{12}) b_1 p_1 b_2 p_2}$$
$$\theta_2^* = \frac{b_2 p_2 [(1 + b_1 p_1) - \xi_{12} b_1 p_1]}{1 + b_1 p_1 + b_2 p_2 + (1 - \xi_{12}) b_1 p_1 b_2 p_2} \tag{36}$$

we are able to obtain qualitative simulations of the experimental observations of Fig. 20. The simulations using Gu *et al.* modification of the extended Langmuir equation are presented in Fig. 21. These simulations are particularly sensitive to the choice of the "discount" factor and the simulations in Fig. 21 can, at best, be viewed as qualitative in nature. We conclude that the proper simulation of breakthrough reversal places an extra demand on the accuracy of the fit of the adsorption isotherm. Accurate multicomponent isotherm parameters are required.

CONCLUSIONS

By comparing experimental breakthrough curves with simulations on the basis of single-component diffusivity and equilibrium data we have been able to verify the predictive capability of the Maxwell–Stefan single file diffusion model. The predictions of this model are more accurate than those of models based on a constant Fick matrix of diffusion coefficients; this conclusion is in agreement with the conclusions of Farooq and Ruthven (1991b).

The predictive capability of the Maxwell–Stefan model has been tested under conditions of co-adsorption, co-desorption and counter-sorption. Even the behaviour of ternary mixtures could be predicted on the basis of single-component information. For breakthrough of propane/propene on Takeda CMS the phenomenon of roll-up reversal was observed but the results could not be simulated entirely satisfactorily as the rest of the simulations in this paper because of inadequate accuracy of the multicomponent adsorption isotherm.

NOTATION

b_i parameter in the Langmuir adsorption isotherm, kPa^{-1} or Pa^{-1}
$[B]$ matrix of inverted Maxwell–Stefan diffusivities, $m^{-2}\,s$
c_0 inlet (at $z = 0$) molar concentration of the fluid mixture, $mol\,m^{-3}$
c molar concentration of the fluid mixture, $mol\,m^{-3}$
c_i molar concentration of species i, $mol\,m^{-3}$
d_p particle diameter, m
D Fick diffusivity in binary mixture, $m^{-2}\,s^{-1}$
$[D]$ matrix of Fick diffusivities for multicomponent system, $m^2\,s^{-1}$
$Đ_{ij}$ Maxwell–Stefan counter-sorption diffusivity, $m^2\,s^{-1}$
$Đ_i$ Maxwell–Stefan diffusivity of component i, $m^2\,s^{-1}$
$Đ_i(0)$ Maxwell–Stefan diffusivity at zero coverage, $m^2\,s^{-1}$
$Đ_{i,\mathrm{eff}}$ Maxwell–Stefan diffusivity of component i, $m^2\,s^{-1}$
D_{12}^M molecular gas diffusivity, $m^2\,s^{-1}$
E axial dispersion coefficient, $m^2\,s^{-1}$
f_i fugacity of species i ($= p_i$ for ideal gases), Pa
Fo Fourier number [$4Đ\,t/d_p^2$ (single particle)]
k_f external film mass transfer coefficient, $m\,s^{-1}$
L length of column, m
n number of diffusion species
$\mathbf{N}_i$ molar flux of species i, $mol\,m^{-2}\,s^{-1}$
p system pressure, Pa
p_i partial presure of species i, Pa
P_{sat} saturation vapour pressure, Pa
Pe Peclet number ($= u_0 L/E$)
q_i adsorbed species concentration within micropores, $mol\,kg^{-1}$
q_{sat} total saturation concentration of adsorbed species, $mol\,kg^{-1}$
q^* equilibrium concentration of adsorbed species, $mol\,kg^{-1}$
r radial distance coordinate, m
R gas constant, $8.314\,J\,mol^{-1}\,K^{-1}$
Re Reynolds number
S_A apparent surface area, $m^2\,g^{-1}$
Sc Schmidt number
t time, s
T absolute temperature, K
u interstitial gas velocity, $m\,s^{-1}$
u_0 interstitial gas velocity at inlet ($z = 0$), $m\,s^{-1}$
$\mathbf{v}_i$ velocity of the diffusing species i, $m\,s^{-1}$
V_p pore volume per unit mass of adsorbent, $cm^3\,g^{-1}$
x_i mole fraction of species i
z direction coordinate, m
z number of nearest neighbour vacant sites

Greek letters

Γ thermodynamic correction factor for binary mixture
$[\Gamma]$ matrix of thermodynamic factors
δ length of diffusion path or thickness of membrane, m
δ_{ij} Kronecker delta ($= 1$ for $i = j$, $= 0$ for $i \neq j$)
ε porosity of particle
ε_b void fraction of adsorbent bed
θ_i fractional surface occupancy of component i
θ_t total surface occupancy of n species
$\theta_{i,\mathrm{sat}}$ fractional surface occupancy of component i at saturation
θ_V fraction of unoccupied sites
λ lateral displacement, m
μ_i molar chemical potential, $J\,mol^{-1}$
ν_i jump frequency of component i, s^{-1}
ζ_{ij} discount factor
ρ particle density, $kg\,m^{-3}$
τ dimensionless time ($= u_0 t/L$)

Subscripts

eff effective parameter
i, j referring to components in mixture
I referring to inert
sat parameter value at saturation
t referring to total
0 referring to position $z = 0$
$n + 1$ referring to pseudo-species

Superscripts

* equilibrium value
0 standard state
— overbar denotes averaged value

REFERENCES

Farooq, S. and Ruthven, D. M., 1991a, Dynamics of kinetically controlled binary adsorption in a fixed bed. *A.I.Ch.E. J.* **37**, 299–301.

Farooq, S. and Ruthven, D. M., 1991b, Numerical simulation of kinetically controlled pressure swing adsorption

bulk separation based on a diffusion model. *Chem. Engng Sci.* **46**, 2213–2224.
Froment, G. F. and Bischoff, K. B., 1990, *Chemical Reactor Analysis and Design*, 2nd Edition. Wiley, New York.
Gu, T., Tsai, G.-J. and Tsao, G. T., 1991, Multicomponent adsorption and chromatography with uneven saturation capacities. *A.I.Ch.E. J.* **37**, 1333–1340.
Habgood, H. W., 1958, The kinetics of molecular sieve action. Sorption of nitrogen–methane mixtures by Linde molecular sieve 4A. *Can. J. Chem.* **36**, 1384–1397.
Kapteijn, F., Bakker, W. J. W., Zheng, G. *et al.*, 1994a, The temperature and occupance dependent diffusion of *n*-butane through a silicalite membrane. *Microporous Materials* (to be published).
Kapteijn, F., Bakker, W. J. W., Zheng, G. *et al.*, 1994b, Permeation and separation of light hydrocarbons through a silicalite-1 membrane. Application of the generalized Maxwell–Stefan theory. *Chem. Engng. J.* (to be published).
Kärger, J. and Ruthven, D. M., 1992, *Diffusion in Zeolites*. Wiley, New York.
Krishna, R., 1990, Multicomponent surface diffusion of adsorbed species: a description based on the generalized Maxwell–Stefan equations. *Chem. Engng Sci.* **45**, 1779–1791.
Krishna, R., 1993a, Problems and pitfalls in the use of the Fick formulation for intraparticle diffusion. *Chem. Engng Sci.* **48**, 845–861.
Krishna, R., 1993b, A unified approach to the modelling of intraparticle diffusion in adsorption processes. *Gas Separ. Purif.* **7**, 91–104.
Mason, E. A. and Malinauskas, A. P., 1983, *Gas Transport in Porous Media: The Dusty Gas Model*. Elsevier, Amsterdam.
Qureshi, W. R. and Wei, J., 1990, One- and two-component diffusion in zeolite ZSM-5. I. Theoretical. *J. Catal.* **126**, 126–146.
Rao, M. B. and Sircar, S., 1993, Nanoporous carbon membrane for gas separation. *Gas Separ. Purif.* **7**, 279–284.
Reed, D. A. and Ehrlich, G., 1981, Surface diffusion, atomic jump rates and thermodynamics. *Surf. Sci.* **102**, 588–609.
Riekert, L., 1971, Rates of adsorption and diffusion of hydrocarbons in zeolites. *A.I.Ch.E. J.* **17**, 446–454.
Round, G. F., Hadgood, H. W. and Newton, R., 1966, A numerical analysis of surface diffusion in a binary adsorbed film. *Separ. Sci.* **1**, 219–244.
Ruthven, D. M., 1984, *Principles of Adsorption and Adsorption Processes*. Wiley, New York.
Ruthven, D. M., Farooq, S. and Knaebel, K. S., *Pressure Swing Adsorption*. VCH Publishers, New York.
Schiesser, W. E., 1991, *The Numerical Methods of Lines: Integration of Partial Differential Equations*. Academic Press, San Diego.
Vignes, A., 1966, Diffusion in binary solutions. *Ind. Engng Chem. Fundam.* **5**, 189–199.
Wakao, N. and Funazkri, T., 1978, Effect of fluid dispersion coefficients on particle-to-fluid mass transfer coefficients in packed beds. *Chem. Engng Sci.* **33**, 1375–1384.
Wakao, N., Kaguei, S. and Nagai, H., 1978, Effective diffusion coefficients for fluid species reacting with first order kinetics in packed bed reactors and discussion on evaluation of catalyst effectiveness factor. *Chem. Engng Sci.* **33**, 183–187.
Wesselingh, J. A. and Krishna, R., 1990, *Mass Transfer*. Ellis Horwood, Chichester.
Yang, R. T., 1987, *Gas Separation by Adsorption Processes*. Butterworths, Boston.
Yang, R. T., Chen, Y. D. and Yeh, Y. T., 1991, Predictions of cross-term coefficients in binary diffusion: diffusion in zeolite. *Chem. Engng. Sci.* **46**, 3089–3099.
Zhdanov, V. P., 1985, General equations for description of surface diffusion in the framework of the lattice-gas model. *Surf. Sci.* **149**, L13–L17.